Composites: Part A 192 (2025) 108802

Contents lists available at ScienceDirect

Composites Part A

journal homepage: www.elsevier.com/locate/compositesa

Enhancing the thermal conductivity and dielectric properties of polymer composite film through segregated boron nitride nanosheets☆

Miracle Hope Adegun [a], Kit-Ying Chan [b], Heng Zhang [b], Yunfei Yang [b], Xiaomeng Zhao [b], Xuili Dong [b], Xi Shen [b,c,*], Jinglei Yang [a], Jang-Kyo Kim [d,*]

[a] Department of Mechanical and Aerospace Engineering, The Hong Kong University of Science and Technology, Clearwater Bay, Kowloon, Hong Kong
[b] Department of Aeronautical and Aviation Engineering, The Hong Kong Polytechnic University, Hung Hom, Kowloon, Hong Kong
[c] The Research Institute for Sports Science and Technology, The Hong Kong Polytechnic University, Hung Hom, Kowloon, Hong Kong
[d] School of Mechanical and Manufacturing Engineering, The University of New South Wales, Sydney, NSW 2052, Australia

HIGHLIGHTS

- Segregated and aligned BNNS in PVA matrix are achieved using sequential freeze-casting.
- The sequential freeze-casting involves infiltrating BNNS into the micro-channels of PVA aerogel followed by hot pressing.
- The unique structure yields 267% higher thermal conductivity than conventional composites with dispersed BNNS.
- The nanocomposite films possess high in-plane thermal conductivity, good electrical resistivity, and low dielectric loss.
- These unique properties make the composite film an ideal candidate for heat dissipation in microelectronics.

GRAPHICAL ABSTRACT

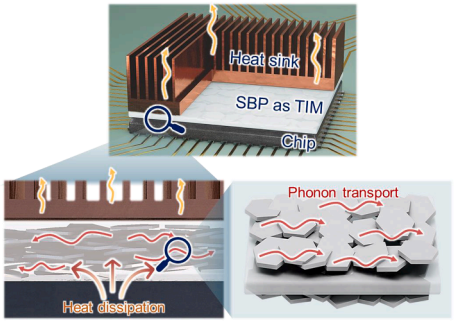

ARTICLE INFO

Keywords:
Boron nitride nanosheets
Freeze-casting
Thermal conduction
Interfacial thermal resistance
Dielectric loss

ABSTRACT

High interfacial thermal resistance (ITR) between thermally conductive nanofillers and polymer matrix, and lack of good orientation of nanofillers are primary limiting factors in harnessing their inherent thermal conductivity in polymer nanocomposites. Thus, exploiting ultrahigh thermal conductivities of nanofillers involves developing methods or mechanisms that can minimize the ITR. In this work, boron nitride nanosheets (BNNS)/polyvinyl alcohol (PVA) nanocomposite films with segregation-induced interconnection among BNNS are fabricated by a sequential unidirection freeze-casting (UFC) technique. A PVA aerogel is first made by UFC followed by infiltrating functionalized BNNS into its pores and microchannels which is subjected to a second UFC process. The composite aerogel is subsequently hot pressed to compact the available pore channels for reduced ITR arising from better contact between the segregated BNNS cell walls. The resulting segregated BNNS/PVA (SBP) nanocomposite film with 40 wt% BNNS exhibits high thermal conductivity of 5.2 W/mK, which is about 267 % higher

☆ This article is part of a special issue entitled: 'Tribute to Adrian Mouritz' published in Composites Part A.

* Corresponding authors.
E-mail addresses: xi.shen@polyu.edu.hk (X. Shen), jangkyo.kim@unsw.edu.au (J.-K. Kim).

https://doi.org/10.1016/j.compositesa.2025.108802
Received 15 October 2024; Received in revised form 21 January 2025; Accepted 11 February 2025
Available online 12 February 2025

than the nanocomposite film containing dispersed BNNS made by conventional UFC. The SBP film also possessed high electrical insulation characteristics and a very low dielectric loss of 10^{-2} at a frequency of 1 kHz, properties arising directly from the segregated BNNS. The sequential UFC provides an effective method to incorporate aligned and interconnected BNNS through segregation for enhanced thermal conductivity and electrical resistivity for thermal management in microelectronics and integrated circuits.

1. Introduction

The ever-increasing heat generation from power microelectronics and electronic devices as a result of miniaturization necessitate efficient thermal management to dissipate the heat so as to ensure their performance, safety and extended service life [1–5]. Conventional metals with high thermal conductivities (TCs) and their composites are not suitable for these applications because of their high densities, rigid structures and high electrical conductivities. Thus, polymer-based composites are considered alternatives, thanks to their lightweights, flexibility, low costs and ease of processing [6–9]. The majority of polymers possess very low TCs, often below 0.5 W/mK [10,11], thus requiring reinforcement of thermally conducting fillers for heat dissipation [1,12]. Thermal interface materials (TIM) must possess a minimum TC of 1 W/mK [13]. Many different materials have been explored as composite fillers to enhance TCs of polymer composites: they include carbon-based nanomaterials, such as graphene [13,14] and carbon nanotubes [15], MXene [16], and metallic nanoparticles (NPs), such as Cu NPs [17] and Ag NPs[18,19], and ceramics fillers like boron nitride (BN) [2,20–22], silicon nitride (Si_3N_4) [23], aluminum nitride (AlN) [24], magnesium oxide (MgO) [25], alumina (Al_2O_3) [24], zinc oxide (ZnO) [26] and silicon carbide (SiC) [27]. These nanofillers have been incorporated as single or hybrid nanofillers comprising a mixture of carbon and ceramic-based fillers. However, the drawback of hybrid structures consisting of carbon-based fillers lies in their high electrical conductivities [28]. Moreover, the large interfacial thermal resistance (ITR) between fillers and polymer matrices because of phonon mismatch at their interfaces is the key limiting factor to improve TCs of composites [5,29]. Therefore, efforts have been continuously made through developing or modifying fabrication processes and designing new composite structures to ensure that the promising thermal properties stemming from the nanofillers are better harnessed without sacrificing the electrical insulation properties [7,11,30]. These approaches are centred around reducing the ITR between the nanofillers and matrix and enhancing the orientation of nanofillers within the composite by using ceramic nanofillers [31].

In order to reduce the ITR while enhancing the reinforcing effect of nanofillers in the polymeric matrix, nanofillers are often functionalized to improve their adhesion with the polymer. The composites with functionalized nanofillers were reported to possess higher TCs than the non-functionalized counterparts [32,33]. The alignment of 2D nanofillers in the polymer matrix is another positive approach minimizing the resistance of phonon transport by utilizing the high in-plane TCs. Several

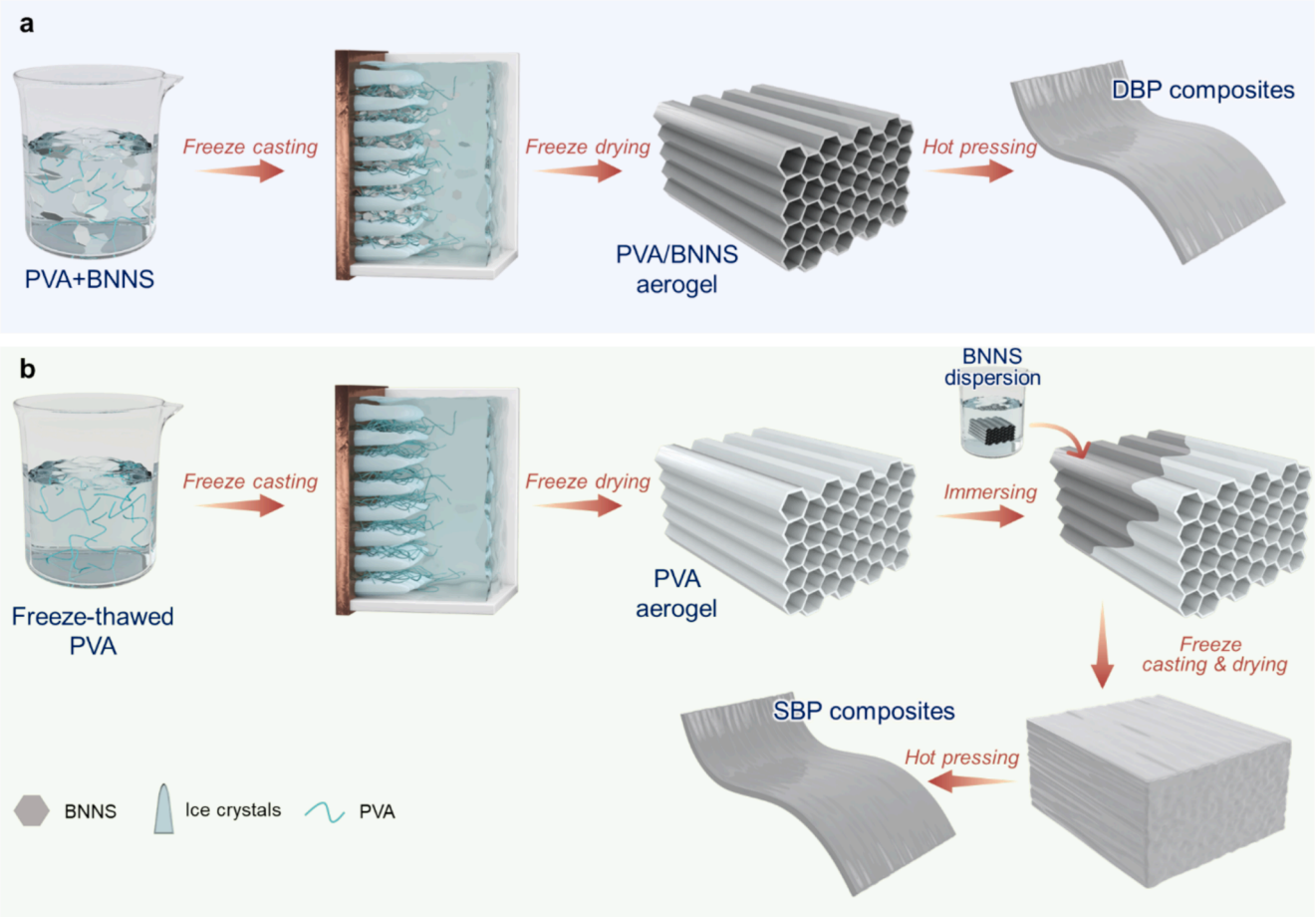

Fig. 1. Schematic diagram illustrating the fabrication of nanocomposite aerogels using (a) one-pot UFC and (b) sequential UFC, followed by compaction to produce DBP and SBP composites films, respectively.

enabling techniques have been devised for the alignment of nanofillers, such as electrospinning [2,21], magnetic alignment [34–36], application of electric field [37], unidirectional freeze casting (UFC) [3,14,38,39], infiltration [14,40], shear force [41] and vacuum-assisted filtration [42–44]. UFC, in particular, exploits the ice crystals grown from the cold source as templates to realize ordered 3D structures containing anisotropic pores using an aqueous solution containing nanofillers [7]. The technique has been adopted for directional heat dissipation or heat insulation, thereby preventing heat localization in the composite [45–47]. However, the conventional UFC uses mixture solution of 2D nanofillers and matrix for freeze-casting, resulting in dispersed nanofillers which are physically separated by the polymer matrix (Fig. 1a). This inevitably imposes significant ITR. A new technique based on UFC is needed to allow direct interconnection between 2D nanofillers so that the TC of composite can be further improved.

Here, we develop a sequential freeze-casting technique to fabricate a BNNS/polyvinyl alcohol (PVA) composite film with highly aligned and segregated BNNS in the PVA matrix. BNNS is chosen due to its useful properties, such as inherently high TC of about 400 W/mK, good electrically insulating properties, low coefficient of thermal expansion, excellent antioxidation and flame retardant characteristics [7,30,38,48–50]. Distinctively different from the conventional freeze-casting where mixed solution of fillers and matrix is used (Fig. 1a), our technique first construct a neat PVA aerogel with highly-aligned, porous structure by UFC, and BNNS were infiltrated through the microchannels in a second UFC (Fig. 1b). After freeze-drying and compaction, BNNS were segregated in between PVA matrix, giving rise to direct physical contact between individual BNNS and thus reducing the ITR. The TC of segregated composite was 267 % higher than dispersed BNNS/PVA composite made by conventional UFC, reaching 5.2 W/mK in the in-plane direction [51]. The segregated composite film also possessed high electrical insulation characteristics and a very low dielectric loss of 10^{-2} at a frequency of 1 kHz, properties arising directly from the BNNS and potentially useful for applications in integrated circuits and storage systems that requires a dielectric loss below 0.015.

2. Experimental methods

2.1. Exfoliation of BNNS

Hexagonal boron nitride (*h*-BN, 325 mesh and 99.5 %) was supplied by Alfa Aesar. BNNS were exfoliated from *h*-BN and simultaneously functionalized according to our previous work [45] based on an urea-assisted ball-milling process which minimized the mechanical stress on the BNNS lattice [52]. *h*-BN powders and urea at a weight ratio of 1:60 were put in a planetary ball mill and reacted at 400 rpm for 24 hr. Subsequently, the ball-milled mixture was dispersed in deionized (DI) water and centrifugated at 2000 rpm for 20 min. To eliminate any unreacted urea, the supernatant was washed four times at 10000 rpm with DI water before being freeze-dried to produce 2D BNNS. The schematic for the exfoliation of BNNS is shown in Fig. S1.

2.2. Fabrication of BNNS/PVA nanocomposite aerogels and films

To understand the effect of BNNS distribution on the resulting thermal conductivity, two UFC processes were adopted to fabricate the composite films with completely different morphologies, as shown in Fig. 1. In both approaches, BNNS of a predetermined weight percentage (10, 20, 30 and 40 wt%) were added to the PVA solution with a concentration of 25 mg/ml. The designation of the nanocomposite films prepared from both processes is shown in Table 1. The samples were fabricated using either one-pot or sequential UFC technique, which created a large temperature gradient for directional ice growth using liquid nitrogen as coolant. The composite monolith was then dried in a freeze-drying machine at a pressure of 3 Pa, yielding anisotropic cellular pore structure. The two UFC techniques are discussed in Section 3.1.

Table 1
Designations and Constituents of BNNS/PVA Nanocomposite Films.

PVA Concentration (mg/ml)	BNNS Incorporation Method	BNNS Content (wt%)	Designation
25	One-pot UFC	0	Neat PVA
		10	DBP10
		20	DBP20
		30	DBP30
		40	DBP40
	Sequential UFC	10	SBP10
		20	SBP20
		30	SBP30
		40	SBP40

2.3. Characterization and Measurements

The exfoliated BNNS were examined by the Raman spectroscopy (RamanMicro300, Perkin Elmer) while the chemical compositions of *h*-BN, BNNS and PVA were evaluated by the Fourier transform infrared spectroscopy (FTIR, Bruker Vertex 70 Hyperion 1000) over a frequency range of 400 – 4000 cm^{-1}. The morphologies of the composite films and BNNS were characterized using scanning electron microscopes (SEM JEOL JSM-6390 and JSM-6700F) and their chemical compositions were examined using the energy dispersive spectroscopy (EDX). The thickness and lateral size of BNNS were estimated by the atomic force microscopy (AFM, Nanoscope Illa/Dimension 3100) while their crystal structures were characterized by the X-ray diffraction (XRD) analysis. The TCs of the composite films were determined using the thermal constant analyzer (TPS 2500S, Hot Disk) at room temperature based on the transient plane source of anisotropic mode using ~ 0.68 mm thick samples [46]. Four samples from each composition were tested and the average result was reported. The thermal performance was also measured using a thermocouple inserted in a closed chamber, which was placed on a hot plate. The electrical resistance, dielectric constant and dielectric loss were measured on an inductance (L), capacitance (C), and resistance (R) (LCR) meter at a frequency of 1 kHz.

3. Result and Discussion

3.1. Design of nanocomposite film with aligned and segregated BNNS

The fabrication processes for BNNS/PVA composite films are shown in Fig. 1. In the conventional one-pot UFC approach (Fig. 1a), functionalized BNNS and PVA precursor were mixed in DI water at 90 °C to form a homogeneous dispersion, which was then followed by freeze-casting and freeze-drying to obtain BNNS/PVA composite aerogels. Hot pressing the composite aerogels at 20 Psi and 150 °C yielded nanocomposite films, which we designated as dispersed BNNS/PVA (DBP) film because BNNS were dispersed in the PVA matrix due to the pre-mixing of BNNS and PVA before the freeze-casting process.

To achieve interconnected BNNS and thus reduced ITR, we developed a sequential UFC approach (Fig. 1b) involving two-step UFC with each constituent incorporated separately. Neat PVA solution was first freeze-cast and freeze-dried to form PVA aerogels with aligned microchannels and open pores. Subsequently, BNNS solution was infiltrated into the microchannels of the PVA aerogel by osmotic active absorption, which was freeze-cast followed by freeze-drying once more to form composite aerogels. The above two-step UFC was aimed to form segregated BNNS on the pre-formed PVA aerogel skeleton in an effort to create highly interconnected BNNS networks within the PVA matrix in the final product. The aerogels were hot pressed to form nanocomposite films under the same condition as the first approach, designating segregated BNNS/PVA (SBP) films. Both DBP and SBP composite films contained aligned BNNS in the freeze-casting direction. However, a major difference lies in the distribution of BNNS in the PVA matrix. For DBP, BNNS was dispersed in the PVA solution before freeze-casting,

resulting in a spatially uniform distribution of BNNS within PVA. For SBP, by contrast, BNNS was dispersed in DI water before infiltration into a neat PVA aerogel to form highly segregated BNNS. This approach resulted in BNNS aligning on the surfaces of PVA walls, ultimately giving rise to spatially interconnected BNNS networks in the PVA matrix after hot pressing.

3.2. Morphologies and properties of nanocomposite films

The morphologies and other chemical and crystallographic properties of exfoliated BNNS are shown in Fig. S2. The SEM image (Fig. S2a) indicates lateral sizes of BNNS at several hundred nanometers. The shift in Raman peak from 1364 to 1366 cm^{-1} after exfoliation (Fig. S2b) can be attributed to weakened interactions between the individual BNNS, confirming exfoliation of bulk *h*-BN into few layers of nanosheets [53]. The FTIR spectra (Fig. S2c) reveals additional peaks at 1677 and 3340 cm^{-1} in the BNNS spectrum, corresponding to N–H vibration and thus confirming the introduction of amino ($–NH_2$) functional groups on BNNS during ball milling [54]. The $–NH_2$ group enhanced the dispersion of BNNS in water. The XRD spectra (Fig. S2d) show identical peaks at 26.8° and 55.3°, but the broader and lower-intensity (002) peak of BNNS than the *h*-BN counterpart indicates thin BN sheets further confirming successful exfoliation of BNNS [52].

The morphologies of PVA aerogel before incorporating BNNS during the sequential UFC are shown in Fig. 2a and e. Fig. 2a presented aligned PVA cell walls and transversely connecting ligaments. The width of the microchannels formed between the cell walls was less than 10 μm and extended along the freezing direction. The top-view SEM image (Fig. 2e) showed the presence of open pores in the PVA cell walls.

The neat PVA aerogels were hot pressed to form PVA films of thickness ~ 14 % of the aerogels before compaction (Fig. S3). The pores were eliminated after compaction, showing stacked layers of PVA microsheets resembling that of nacre (Fig. 2b). The open pores on the top surface were also consolidated after hot pressing, as shown in Fig. 2f. Similar layered structure was observed in the DBP film containing 40 wt % BNNS, as shown in Fig. 2c. The BNNS were dispersed randomly and sandwiched between PVA matrix layers as a result of solution mixing before UFC. The top-view SEM image of DBP film showed rougher surfaces than the neat PVA film because of the inclusion of BNNS. The SBP film of the same BNNS loading of 40 wt% presented much similar cross-sectional and top-surface morphologies to those of the DBP film, as shown in Fig. 2d and 2 h. In general, however, SBP40 exhibited better closure of cell wall nanopores than the DBP counterpart, as shown in the high magnification SEM images of DBP40 and SBP40 (Fig. S4). The corresponding SEM images of the DBP and SBP films with other compositions are shown in Fig. S5 and S6, respectively. The DBP films retained their inherent layered structures originating from the UFC process, whereas the SBP films showed more closely packed structures than the DBP films because of the segregation of BNNS.

The segregated structure was further confirmed by analyzing compositional differences between DBP40 and SBP40 by the energy dispersive X-ray (EDX) mapping (Fig. S7). The top-view EDX mapping images show that more BNNS appeared in the SBP than DBP films, as indicated by the higher intensities for B and N elements in the former.

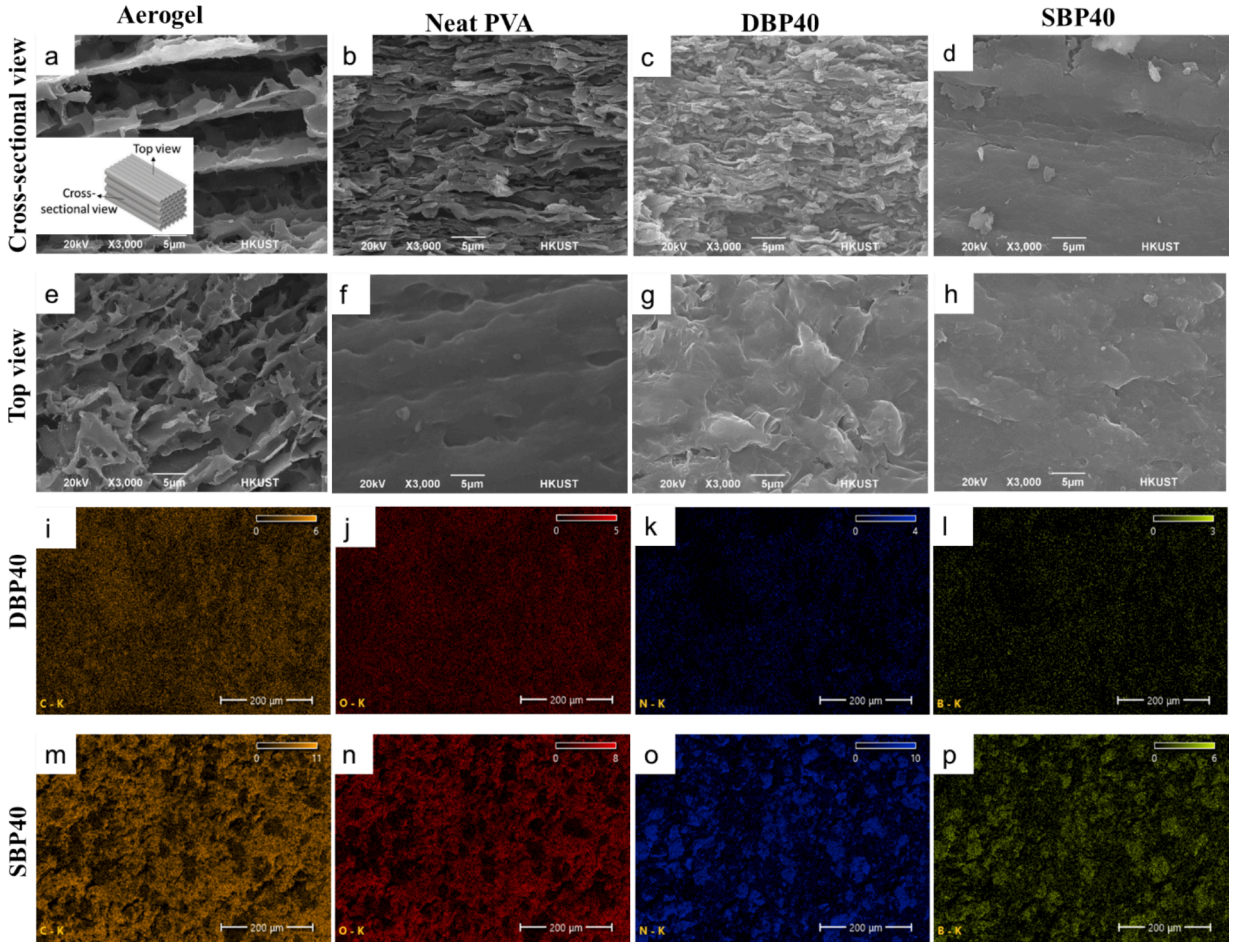

Fig. 2. SEM images showing the (a-d) cross-sectional views and (e-h) top views of (a, e) PVA aerogel; (b, f) PVA film; (c, g) DBP film; and (d, h) SBP film. EDX maps of the top-view SEM images showing relative elemental compositions for the (i – l) DBP and (m – p) SBP films. The mapping images of C, O, N and B are shown in (i, m), (j, n), (k, o), and (l, p), respectively.

Similarly, the cross-sectional elemental maps shown in Fig. 2i-2p also confirm that the B and N elements were more abundant in the SBP than the DBP films. These observations serve as evidence that the BNNS were segregated in the SBP film whereas those in the DBP were dispersed. The distributions of other elements like C and O were essentially similar between the two films.

3.3. TCs of composite films

The TCs of the DBP and SBP films were measured in the in-plane and through-the-thickness directions, as shown in Fig. 3a. The TCs of both films increased with increasing BNNS loading, and significant anisotropy was observed with much higher in-plane values than those in the through-the-thickness direction. The SBP films showed consistently higher in-plane TCs than the DBP films, reaching 5.20 W/mK at 40 wt% of BNNS, about 15 times that of the neat PVA film. In comparison, the TC of DBP film of the same BNNS loading was only 1.95 W/mK.

The higher TC of SBP than DBP can be explained by the completely different distributions of BNNS fillers, as illustrated in Fig. 3b. The DBP films were fabricated by UFC of BNNS dispersed in the PVA matrix to form composite aerogels which were subjected to freeze-drying and hot pressing. Thus, it is envisaged that the functionalized BNNS were uniformly dispersed in the PVA matrix, and the thermal transport in the DBP film was therefore mainly through the BNNS-PVA interfaces. These structural features of the DBP composite film limit the phonon transport in the plane direction because of the high ITR between the individual BNNS and PVA, although they were reasonably well aligned in the in-plane direction because of UFC and hot pressing.

In sharp contrast, the SBP films were made by infiltration of BNNS solution into the microchannels created in the neat PVA aerogel. Thus, the BNNS were assembled onto the PVA cell walls, giving rise to segregated BNNS in the PVA matrix after hot pressing. This segregated structure offered continuous nanofiller conducting pathways as phonons were transported through the interconnected BNNS [55–58]. The thermal contact resistance among the segregated BNNS was much lower than that between BNNS and PVA, generating less resistance to phonon transport and thus much higher TCs of SBP than DBP films. To confirm the effect of BNNS distribution on ITR, ITR of both films were predicted based on the Foygel's model and the effective medium theory (EMT) [20], whose details are provided in Supporting Information. The SBP film's ITR was estimated to be 1.6×10^{-9} m^2K/W, which was only about half of the DBP film of 2.8×10^{-9} m^2K/W (Fig. S8). The lower ITR of SBP than DBP substantiates the positive effect of interconnected BNNS in promoting interfacial thermal transport, ultimately translating into a much higher in-plane TC of the SBP films.

Given the unique segregated and aligned BNNS layers in the PVA matrix which is analogous to a unidirectional fiber composite consisting of continuous fibers and a matrix whose overall properties are the result of the volumetric or weighted average of the individual components, we adopted the rule of mixtures (RoM) to predict the TC of the composite according to Equation (1).

$$\lambda_c = \lambda_m(1-V_f) + \left(\frac{\lambda_b}{1+\lambda_b\frac{C_k}{d}}\right)^* V_f \quad (1).$$

where λ_m is the TC of PVA, λ_b is the effective TC of BNNS, d is the thickness of BNNS, and C_k is the ITR among BNNS [59]. The conduction between BNNS and PVA was assuming to be negligible so that phonons were transported mainly through the BNNS networks. Fig. 3c shows the comparison between the experimental and theoretical TCs obtained from the model. Only considering the ITR between BNNS yielded good agreement between the experiment and prediction, partly confirming the advantage of segregated BNNS structure in the SBP films.

The practical thermal dissipation performance of the films was also evaluated by monitoring the temperature changes of the films placed on

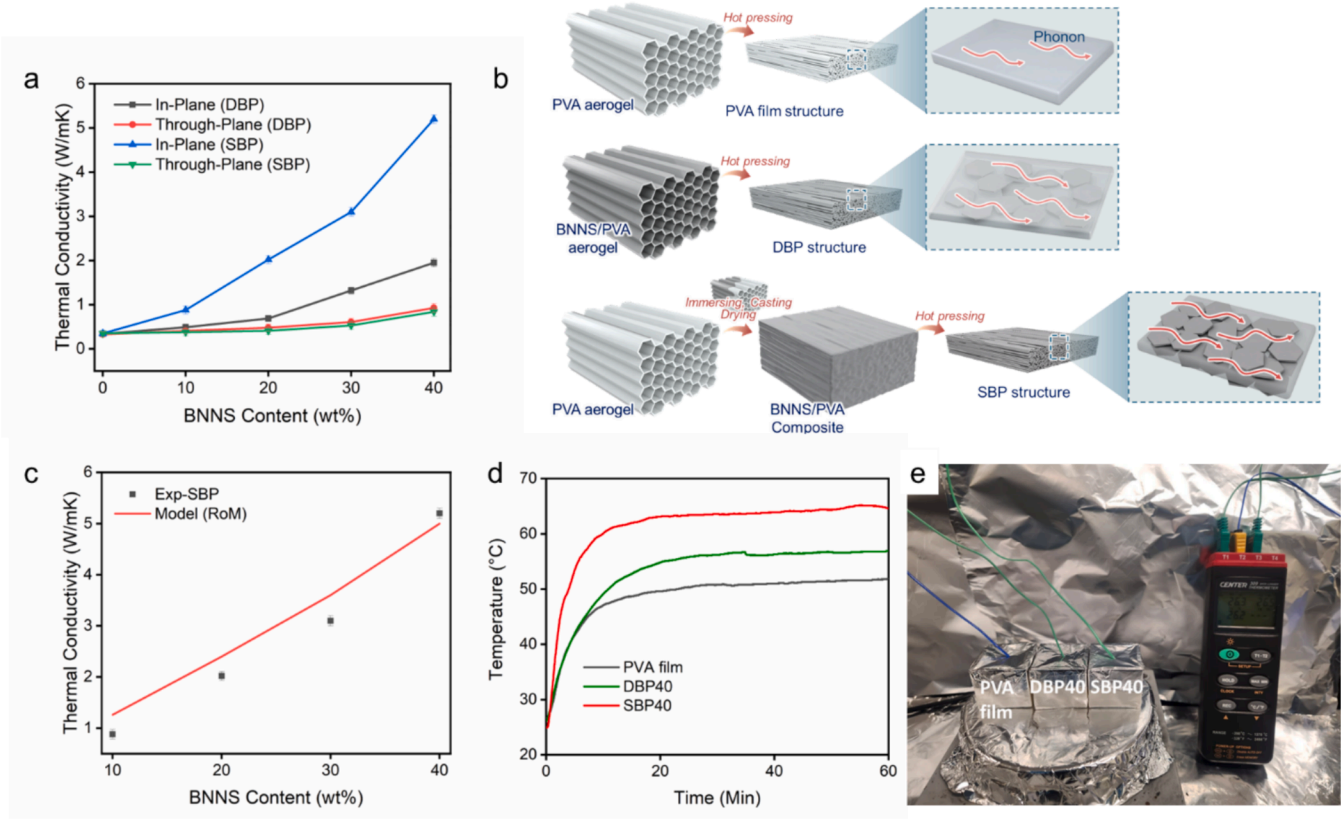

Fig. 3. Thermal properties of BNNS nanocomposite films. (a) TC of composite films; (b) schematics of thermal transport mechanisms in PVA film and DBP and SBP nanocomposite films; (c) comparison between experimental and theoretical TCs for SBP nanocomposite films; (d) variations of temperature of nanocomposite films when placed on a hot plate at 100 °C; (e) setup for thermal performance tests.

a hot plate at 100 °C, as shown in Fig. 3d. The digital image of the experimental setup is shown in Fig. 3e while the schematic representation of the setup is shown in Fig. S9. The SBP film attained a higher temperature in a shorter period of time than both the DBP and pristine PVA film counterparts. Further, the SBP film showed 26.0 % and 14.6 % higher saturated temperatures than those of the PVA and DBP films, respectively. These observations signifies the superior thermal dissipation capacity of the SBP films over their DBP counterparts, indicating the potential for practical thermal management applications [60].

3.4. Dielectric properties

For potential applications of the nanocomposite films as TIMs in electronics, their dielectric properties were also examined, as shown in Fig. 4. Dielectric properties such as dielectric constant, volume resistivity and dielectric loss are crucial for energy storage in electric power systems and advanced electronics [54]. It has been reported that high TCs of dielectric materials imply improved heat dissipation and low potential for thermal runaway, which in turn can contribute to improvement in energy storage capacity [61]. Thus, a good dielectric material is expected to possess excellent electrical resistance and very low dielectric loss [49]. The volume resistivity of PVA film is measured to be 9×10^{12} Ω•cm as shown in Fig. 4a. The volume resistivity increased with increasing BNNS content because of the excellent electrically insulating properties of BNNS. Interestingly, the SBP films with 20 wt% and above showed consistently over 40 % higher volume resistivity than the DBP films, as shown in Fig. S10. This is because the SBP composite structure with segregated BNNS offer enhanced electrical resistance than the DBP counterpart in which the BNNS is intertwined with PVA molecule as a result of the solution mixing process before UFC. The SBP film with a BNNS loading of 40 % showed the highest volume resistivity of 3.6×10^{13} Ω•cm.

The dielectric constants of the PVA and nanocomposite films were also examined at 1 kHz, as shown in Fig. 4b and Fig. S11. The PVA film exhibited a low dielectric constant of 1.34. The dielectric constants of the composite films decreased with increasing BNNS loading because of the electrically insulating characteristics of BNNS which offered strong barriers to charge polarization [62]. The DBP films showed higher dielectric constants than SBP films of the same BNNS loading. Despite the relatively low dielectric constants, the introduction of BNNS significantly contributed towards suppression of dielectric loss. Fig. 4c shows the dielectric loss of the SBP and DBP films measured at a frequency of 1 kHz. The dielectric loss values of nanocomposite films containing different BNNS contents are shown in Fig. S12. The SBP film with 40 wt% BNNS exhibited a dielectric loss of about 10^{-2}, which was better than the DBP film and 86 % lower than that of the neat PVA film. The low dielectric loss can be attributed to the exceptional electrically insulating property of BNNS due to its wide bandgap, serving as electrical barriers for charge conduction and leakage current within the composite film [2,14]. A very low dielectric loss is essential for high voltage applications to minimize the heat generated from high-

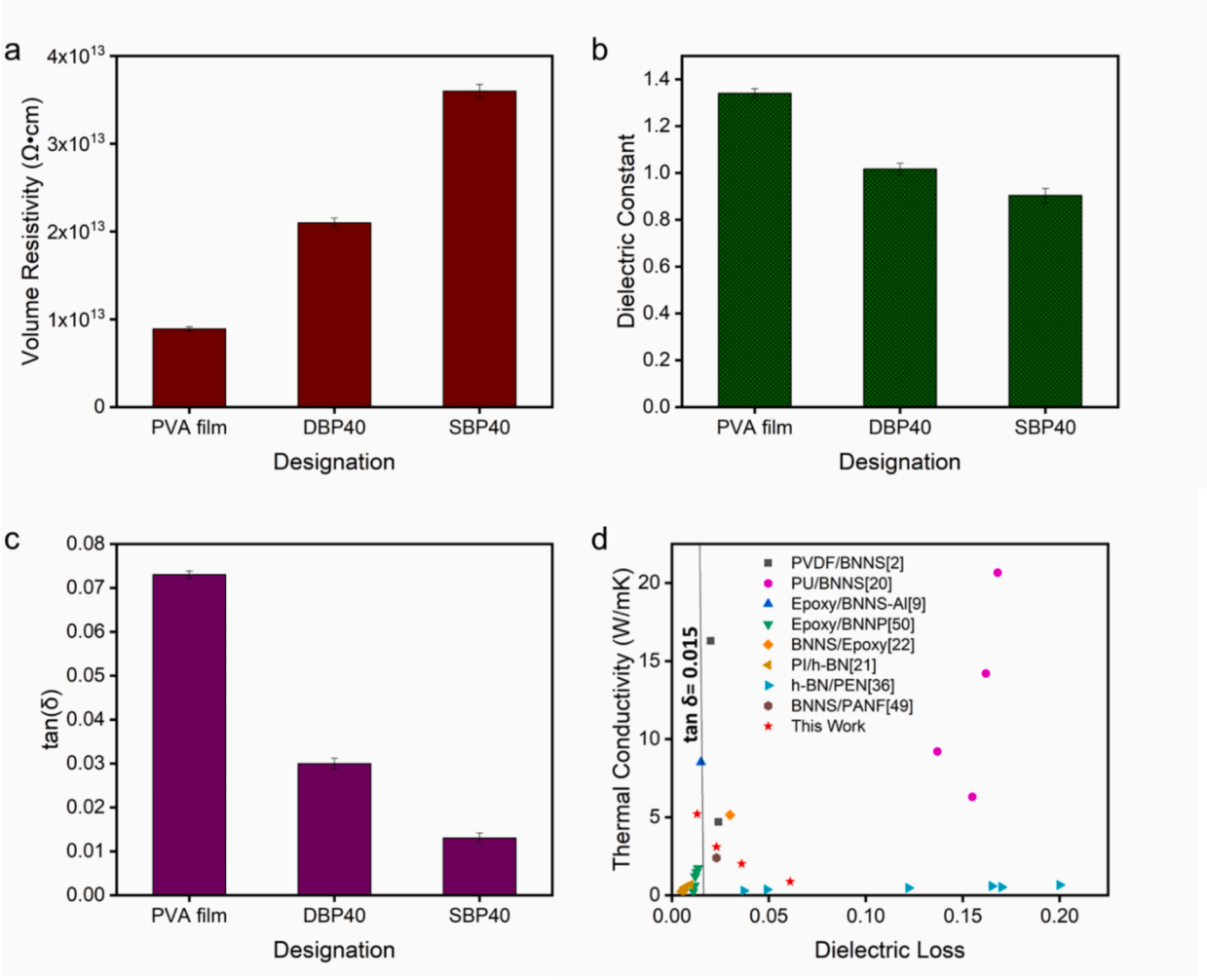

Fig. 4. Electrical and dielectric properties DBP and SBP composite films. (a) Volume resistivity; (b) Dielectric constant; and (c) Dielectric loss of composite films. (d) Comparison of TC and dielectric loss of SBP nanocomposite films with other boron nitride dielectric composites.

frequency alternating currents which often lead to breakdown of dielectrics [63–65].

The dielectric loss and TC of the SBP film with 40 wt% BNNS are compared with other composite films made from BNNS as shown in Fig. 4d. All the composite films, except PU/BNNS [20], were formed by dispersion of *h*-BN, BNNS or boron nitride nanoparticles in the polymer matrix, whereas the PU/BNNS [20] composite was fabricated using heat to spray BNNS on a PU web thereby yielding a structure similar to segregated BNNS within the PU matrix. Although it had a high in-plane TC but its dielectric loss was high, about 10-fold higher than the SBP40 composite film. Further, among the nanocomposite films fabricated by dispersion of BNNS in the polymer matrix, only PVDF/BNNS [2] and Epoxy/BNNS-Al [9] formed by stacking of a number of layers exhibit higher in-plane TC values higher than 6 W/mK. However, their through-thickness TCs are poor, lower than 0.5 W/mK. The SBP40 film showed a higher TC in the through-thickness direction with a low dielectric loss. The high in-plane TC of Epoxy/BNNS-Al [9] was achieved by incorporating alternating layers containing electrically conductive Al. This means that the presence of electrically conductive Al in the matrix may pose a possible electrical short circuit during service. For integrated circuits, energy storage systems and capacitors, a very low dielectric loss of below 0.015 is desired for optimal performance. Thus, the high TC of SBP40 combined with a low dielectric loss can make it an ideal dielectric material for applications in sensor devices, microelectronics, energy storage systems and capacitors.

4. Conclusion

We developed a sequential freeze-casting technique in an effort to induce aligned and segregated BNNS in the PVA matrix for reduced ITR. The SBP nanocomposite films fabricated from infiltration of BNNS into the microchannels created by UFC of neat PVA showed better TC than those fabricated by conventional UFC involving solution mixing of PVA and BNNS. The SBP40 films exhibited a TC of 5.2 W/mK in the in-plane direction, which is about 1400 % improvement over the neat PVA film. This finding was achieved by the presence of interconnected BNNS which offered unimpeded pathways for phonon transport with less thermal resistance. The SBP40 film delivered 26 % enhancement in heat dissipation over the neat PVA film. In addition, the SBP composite film also maintained a dielectric constant close to unity along with excellent suppression of dielectric loss to about 10^{-2}. The excellent TC coupled with enhanced thermal stability, and the very low dielectric loss makes the SBP40 film an excellent candidate for heat dissipation, and as dielectric composites in energy storage devices and capacitors where a very low dielectric loss is required.

CRediT authorship contribution statement

Miracle Hope Adegun: Writing – original draft, Methodology, Formal analysis, Data curation, Conceptualization. **Kit-Ying Chan:** Writing – original draft, Methodology, Data curation, Conceptualization. **Heng Zhang:** Software, Methodology, Formal analysis, Data curation. **Yunfei Yang:** Writing – review & editing, Software, Methodology, Formal analysis, Data curation. **Xiaomeng Zhao:** Methodology, Investigation, Formal analysis. **Xuili Dong:** Methodology, Investigation, Formal analysis. **Xi Shen:** Writing – review & editing, Supervision, Resources, Funding acquisition, Formal analysis, Conceptualization. **Jinglei Yang:** Resources, Formal analysis. **Jang-Kyo Kim:** Writing – review & editing, Supervision, Resources, Funding acquisition, Formal analysis.

Declaration of competing interest

The authors declare that they have no known competing financial interests or personal relationships that could have appeared to influence the work reported in this paper.

Acknowledgements

This project was financially supported by the Young Scientists Fund of National Natural Science Foundation of China (Grant No. 52303106), Research Grants Council of Hong Kong SAR (16200720), Environment and Conservation Fund of Hong Kong SAR (Project No. 21/2022), Research Institute of Sports Science and Technology (Project No. P0043535), Research Institute of Advanced Manufacturing (Project No. P0046125), and the start-up fund for new recruits of PolyU (Project No. P0038855 and P0038858). M.H.A was a recipient of Hong Kong PhD Fellowship Scheme (HKPFS). Technical assistance from the Materials Characterization and Preparation Facility (MCPF), the Advanced Engineering Material Facility (AEMF), and the Environmental Central Facility (ENVF) at HKUST is also appreciated.

Appendix A. Supplementary data

Supplementary data to this article can be found online at https://doi.org/10.1016/j.compositesa.2025.108802.

Data availability

Data will be made available on request.

References

[1] Shen X, Zheng Q, Kim J-K. Rational design of two-dimensional nanofillers for polymer nanocomposites toward multifunctional applications. Prog Mater Sci 2021;115:100708. https://doi.org/10.1016/j.pmatsci.2020.100708.
[2] Chen J, Huang X, Sun B, Jiang P. Highly Thermally Conductive Yet Electrically Insulating Polymer/Boron Nitride Nanosheets Nanocomposite Films for Improved Thermal Management Capability. ACS Nano 2019;13:337–45. https://doi.org/10.1021/acsnano.8b06290.
[3] Zeng X, Yao Y, Gong Z, Wang F, Sun R, Xu J, et al. Ice-Templated Assembly Strategy to Construct 3D Boron Nitride Nanosheet Networks in Polymer Composites for Thermal Conductivity Improvement. Small 2015;11:6205–13. https://doi.org/10.1002/smll.201502173.
[4] Moore AL, Shi L. Emerging challenges and materials for thermal management of electronics. Mater Today 2014;17:163–74. https://doi.org/10.1016/j.mattod.2014.04.003.
[5] Shen X, Wang Z, Wu Y, Liu X, He Y-B, Kim J-K. Multilayer Graphene Enables Higher Efficiency in Improving Thermal Conductivities of Graphene/Epoxy Composites. Nano Lett 2016;16:3585–93. https://doi.org/10.1021/acs.nanolett.6b00722.
[6] Zhang F, Feng Y, Feng W. Three-dimensional interconnected networks for thermally conductive polymer composites: Design, preparation, properties, and mechanisms. Mater Sci Eng R Rep 2020;142:100580. https://doi.org/10.1016/j.mser.2020.100580.
[7] Shen X, Kim J-K. 3D graphene and boron nitride structures for nanocomposites with tailored thermal conductivities: recent advances and perspectives. Funct Compos Struct 2020;2:022001. https://doi.org/10.1088/2631-6331/ab953a.
[8] Hou J, Li G, Yang N, Qin L, Grami ME, Zhang Q, et al. Preparation and characterization of surface modified boron nitride epoxy composites with enhanced thermal conductivity. RSC Adv 2014;4:44282–90. https://doi.org/10.1039/C4RA07394K.
[9] Chen L, Xiao C, Tang Y, Zhang X, Zheng K, Tian X. Preparation and characterization of epoxy-based composite with multilayered structure and high thermal conductivity. Mater Res Express 2019;6:075314. https://doi.org/10.1088/2053-1591/ab1370.
[10] Chae HG, Kumar S. Making Strong Fibers. Science 2008;319:908–9. https://doi.org/10.1126/science.1153911.
[11] Hu D, Liu H, Ma W. Rational design of nanohybrids for highly thermally conductive polymer composites. Compos Commun 2020;21:100427. https://doi.org/10.1016/j.coco.2020.100427.
[12] Feng C-P, Yang L-Y, Yang J, Bai L, Bao R-Y, Liu Z-Y, et al. Recent advances in polymer-based thermal interface materials for thermal management: A mini-review. Compos Commun 2020;22:100528. https://doi.org/10.1016/j.coco.2020.100528.
[13] Shahil KMF, Balandin AA. Graphene–Multilayer Graphene Nanocomposites as Highly Efficient Thermal Interface Materials. Nano Lett 2012;12:861–7. https://doi.org/10.1021/nl203906r.
[14] Guo F, Shen X, Zhou J, Liu D, Zheng Q, Yang J, et al. Highly Thermally Conductive Dielectric Nanocomposites with Synergistic Alignments of Graphene and Boron Nitride Nanosheets. Adv Funct Mater 2020;30:1910826. https://doi.org/10.1002/adfm.201910826.
[15] Cui W, Du F, Zhao J, Zhang W, Yang Y, Xie X, et al. Improving thermal conductivity while retaining high electrical resistivity of epoxy composites by incorporating

silica-coated multi-walled carbon nanotubes. Carbon 2011;49:495–500. https://doi.org/10.1016/j.carbon.2010.09.047.
[16] Li L, Cao Y, Liu X, Wang J, Yang Y, Wang W. Multifunctional MXene-Based Fireproof Electromagnetic Shielding Films with Exceptional Anisotropic Heat Dissipation Capability and Joule Heating Performance. ACS Appl Mater Interfaces 2020;12:27350–60. https://doi.org/10.1021/acsami.0c05692.
[17] Li J, Li X, Zheng Y, Liu Z, Tian Q, Liu X. New underfill material based on copper nanoparticles coated with silica for high thermally conductive and electrically insulating epoxy composites. J Mater Sci 2019;54:6258–71. https://doi.org/10.1007/s10853-019-03335-9.
[18] Wang F, Zeng X, Yao Y, Sun R, Xu J, Wong C-P. Silver Nanoparticle-Deposited Boron Nitride Nanosheets as Fillers for Polymeric Composites with High Thermal Conductivity. Sci Rep 2016;6:19394. https://doi.org/10.1038/srep19394.
[19] Shen Z, Feng J. Highly Thermally Conductive Composite Films Based on Nanofibrillated Cellulose in Situ Coated with a Small Amount of Silver Nanoparticles. ACS Appl Mater Interfaces 2018;10:24193–200. https://doi.org/10.1021/acsami.8b07249.
[20] Du P-Y, Wang Z-X, Ren J-W, Zhao L-H, Jia S-L, Jia L-C. Scalable Polymer-Infiltrated Boron Nitride Nanoplatelet Films with High Thermal Conductivity and Electrical Insulation for Thermal Management. ACS Appl Electron Mater 2022;4:4622–31. https://doi.org/10.1021/acsaelm.2c00858.
[21] Gu J, Lv Z, Wu Y, Guo Y, Tian L, Qiu H, et al. Dielectric thermally conductive boron nitride/polyimide composites with outstanding thermal stabilities via in -situ polymerization-electrospinning-hot press method. Compos Part Appl Sci Manuf 2017;94:209–16. https://doi.org/10.1016/j.compositesa.2016.12.014.
[22] Yuan F, Jiao W, Yang F, Liu W, Xu Z, Wang R. Surface modification and magnetic alignment of hexagonal boron nitride nanosheets for highly thermally conductive composites. RSC Adv 2017;7:43380–9. https://doi.org/10.1039/C7RA08516H.
[23] Zhou W, Wang C, Ai T, Wu K, Zhao F, Gu H. A novel fiber-reinforced polyethylene composite with added silicon nitride particles for enhanced thermal conductivity. Compos Part Appl Sci Manuf 2009;40:830–6. https://doi.org/10.1016/j.compositesa.2009.04.005.
[24] Choi S, Kim J. Thermal conductivity of epoxy composites with a binary-particle system of aluminum oxide and aluminum nitride fillers. Compos Part B Eng 2013;51:140–7. https://doi.org/10.1016/j.compositesb.2013.03.002.
[25] Jung H, Han J-H, Jung I-C. Fabrication of silicone-based gap filler for electric vehicles using magnesium oxide thermally conductive fillers. J Korean Ceram Soc 2024. https://doi.org/10.1007/s43207-024-00403-y.
[26] Zhang Q, Weng Z, Wu K, Chen W, Lu M. A Novel Thermally Conductive Phase Change Material of Polythiophene-Coated Core–Shell Polyethylene Glycol/Nano Zinc Oxide by In Situ Polymerization. J Phys Chem C 2020;124:25202–10. https://doi.org/10.1021/acs.jpcc.0c06749.
[27] Vu MC, Choi W-K, Lee SG, Park PJ, Kim DH, Islam MA, et al. High Thermal Conductivity Enhancement of Polymer Composites with Vertically Aligned Silicon Carbide Sheet Scaffolds. ACS Appl Mater Interfaces 2020;12:23388–98. https://doi.org/10.1021/acsami.0c02421.
[28] Yao Y, Zeng X, Wang F, Sun R, Xu J, Wong C-P. Significant Enhancement of Thermal Conductivity in Bioinspired Freestanding Boron Nitride Papers Filled with Graphene Oxide. Chem Mater 2016;28:1049–57. https://doi.org/10.1021/acs.chemmater.5b04187.
[29] Zhang F, Sun Y, Guo L, Zhang Y, Liu D, Feng W, et al. Microstructural Welding Engineering of Carbon Nanotube/Polydimethylsiloxane Nanocomposites with Improved Interfacial Thermal Transport. Adv Funct Mater 2024;34:2311906. https://doi.org/10.1002/adfm.202311906.
[30] Li P, Wang A, Fan J, Kang Q, Jiang P, Bao H, et al. Thermo-Optically Designed Scalable Photonic Films with High Thermal Conductivity for Subambient and Above-Ambient Radiative Cooling. Adv Funct Mater 2022;32:2109542. https://doi.org/10.1002/adfm.202109542.
[31] Warzoha RJ, Fleischer AS. Heat flow at nanoparticle interfaces. Nano Energy 2014;6:137–58. https://doi.org/10.1016/j.nanoen.2014.03.014.
[32] Wang Z, Yang M, Cheng Y, Liu J, Xiao B, Chen S, et al. Dielectric properties and thermal conductivity of epoxy composites using quantum-sized silver decorated core/shell structured alumina/polydopamine. Compos Part Appl Sci Manuf 2019;118:302–11. https://doi.org/10.1016/j.compositesa.2018.12.022.
[33] Wang Z, Priego P, Meziani MJ, Wirth K, Bhattacharya S, Rao A, et al. Dispersion of high-quality boron nitride nanosheets in polyethylene for nanocomposites of superior thermal transport properties. Nanoscale Adv 2020;2:2507–13. https://doi.org/10.1039/D0NA00190B.
[34] He Y, Kuang F, Che Z, Sun F, Zheng K, Zhang J, et al. Achieving high out-of-plane thermal conductivity for boron nitride nano sheets/epoxy composite films by magnetic orientation. Compos Part Appl Sci Manuf 2022;157:106933. https://doi.org/10.1016/j.compositesa.2022.106933.
[35] Lin Z, Liu Y, Raghavan S, Moon K, Sitaraman SK, Wong C. Magnetic Alignment of Hexagonal Boron Nitride Platelets in Polymer Matrix: Toward High Performance Anisotropic Polymer Composites for Electronic Encapsulation. ACS Appl Mater Interfaces 2013;5:7633–40. https://doi.org/10.1021/am401939z.
[36] Zhan Y, Long Z, Wan X, Zhan C, Zhang J, He Y. Enhanced dielectric permittivity and thermal conductivity of hexagonal boron nitride/poly(arylene ether nitrile) composites through magnetic alignment and mussel inspired co-modification. Ceram Int 2017;43:12109–19. https://doi.org/10.1016/j.ceramint.2017.06.068.
[37] Cho H-B, Nakayama T, Suematsu H, Suzuki T, Jiang W, Niihara K, et al. Insulating polymer nanocomposites with high-thermal-conduction routes via linear densely packed boron nitride nanosheets. Compos Sci Technol 2016;129:205–13. https://doi.org/10.1016/j.compscitech.2016.04.033.
[38] Sun H, Bao Q, Chen G, Wu S, Liu Y, Wang Q. Highly thermal conductive and flame retardant poly(vinyl alcohol) film with synergistic alignments of boron nitride nanosheets/Ti3C2Tx MXene for thermal interface materials. Polymer 2023;283:126277. https://doi.org/10.1016/j.polymer.2023.126277.
[39] Zhao X, Zhang H, Chan K-Y, Huang X, Yang Y, Shen X. Tree-Inspired Structurally Graded Aerogel with Synergistic Water, Salt, and Thermal Transport for High-Salinity Solar-Powered Evaporation. Nano-Micro Lett 2024;16:222. https://doi.org/10.1007/s40820-024-01448-8.
[40] Han J, Du G, Gao W, Bai H. An Anisotropically High Thermal Conductive Boron Nitride/Epoxy Composite Based on Nacre-Mimetic 3D Network. Adv Funct Mater 2019;29:1900412. https://doi.org/10.1002/adfm.201900412.
[41] Zhang X, Zhang J, Xia L, Li C, Wang J, Xu F, et al. Simple and Consecutive Melt Extrusion Method to Fabricate Thermally Conductive Composites with Highly Oriented Boron Nitrides. ACS Appl Mater Interfaces 2017;9:22977–84. https://doi.org/10.1021/acsami.7b05866.
[42] Wu Y, Xue Y, Qin S, Liu D, Wang X, Hu X, et al. BN Nanosheet/Polymer Films with Highly Anisotropic Thermal Conductivity for Thermal Management Applications. ACS Appl Mater Interfaces 2017;9:43163–70. https://doi.org/10.1021/acsami.7b15264.
[43] Zhu H, Li Y, Fang Z, Xu J, Cao F, Wan J, et al. Highly Thermally Conductive Papers with Percolative Layered Boron Nitride Nanosheets. ACS Nano 2014;8:3606–13. https://doi.org/10.1021/nn500134m.
[44] Zhang Y, Zhang G, Ma Z, Qin J, Shen X. Heterogeneous MXene-based films with graded electrical conductivity towards highly efficient EMI shielding and electrothermal heating. Nano Res 2024;17:7264–74. https://doi.org/10.1007/s12274-024-6709-z.
[45] Adegun MH, Chan K-Y, Yang J, Venkatesan H, Kim E, Zhang H, et al. Anisotropic thermally superinsulating boron nitride composite aerogel for building thermal management. Compos Part Appl Sci Manuf 2023;169:107522. https://doi.org/10.1016/j.compositesa.2023.107522.
[46] Chan K-Y, Shen X, Yang J, Lin K-T, Venkatesan H, Kim E, et al. Scalable anisotropic cooling aerogels by additive freeze-casting. Nat Commun 2022;13:5553. https://doi.org/10.1038/s41467-022-33234-8.
[47] Yang J, Chan K-Y, Venkatesan H, Kim E, Adegun MH, Lee J-H, et al. Superinsulating BNNS/PVA Composite Aerogels with High Solar Reflectance for Energy-Efficient Buildings. Nano-Micro Lett 2022;14:54. https://doi.org/10.1007/s40820-022-00797-6.
[48] Yang X, Guo Y, Han Y, Li Y, Ma T, Chen M, et al. Significant improvement of thermal conductivities for BNNS/PVA composite films via electrospinning followed by hot-pressing technology. Compos Part B Eng 2019;175:107070. https://doi.org/10.1016/j.compositesb.2019.107070.
[49] Rahman MM, Puthirath AB, Adumbumkulath A, Tsafack T, Robatjazi H, Barnes M, et al. Fiber Reinforced Layered Dielectric Nanocomposite. Adv Funct Mater 2019;29:1900056. https://doi.org/10.1002/adfm.201900056.
[50] Lee D, Lee S, Byun S, Paik K-W, Song SH. Novel dielectric BN/epoxy nanocomposites with enhanced heat dissipation performance for electronic packaging. Compos Part Appl Sci Manuf 2018;107:217–23. https://doi.org/10.1016/j.compositesa.2018.01.009.
[51] Weng C, Li W, Wu J, Shen L, Yang W, Deng C, et al. Thermal shock exfoliated and siloxane cross-linked graphene framework for high performance epoxy-based thermally conductive composites. J Mater Sci 2021;56:17601–14. https://doi.org/10.1007/s10853-021-06147-y.
[52] Lei W, Mochalin VN, Liu D, Qin S, Gogotsi Y, Chen Y. Boron nitride colloidal solutions, ultralight aerogels and freestanding membranes through one-step exfoliation and functionalization. Nat Commun 2015;6:8849. https://doi.org/10.1038/ncomms9849.
[53] Sainsbury T, Satti A, May P, Wang Z, McGovern I, Gun'ko YK, et al. Oxygen Radical Functionalization of Boron Nitride Nanosheets. J Am Chem Soc 2012;134:18758–71. https://doi.org/10.1021/ja3080665.
[54] Azizi A, Gadinski MR, Li Q, AlSaud MA, Wang J, Wang Y, et al. High-Performance Polymers Sandwiched with Chemical Vapor Deposited Hexagonal Boron Nitrides as Scalable High-Temperature Dielectric Materials. Adv Mater 2017;29:1701864. https://doi.org/10.1002/adma.201701864.
[55] Li A, Zhang C, Zhang Y-F. Thermal Conductivity of Graphene-Polymer Composites: Mechanisms, Properties, and Applications. Polymers 2017;9:437. https://doi.org/10.3390/polym9090437.
[56] Yang J, Shen X, Yang W, Kim JK. Templating strategies for 3D-structured thermally conductive composites: Recent advances and thermal energy applications. Prog Mater Sci 2023;133:101054. https://doi.org/10.1016/j.pmatsci.2022.101054.
[57] Jo I, Pettes MT, Kim J, Watanabe K, Taniguchi T, Yao Z, et al. Thermal Conductivity and Phonon Transport in Suspended Few-Layer Hexagonal Boron Nitride. Nano Lett 2013;13:550–4. https://doi.org/10.1021/nl304060g.
[58] Wang Y, Zhang Z, Li T, Ma P, Zhang X, Xia B, et al. Artificial Nacre Epoxy Nanomaterials Based on Janus Graphene Oxide for Thermal Management Applications. ACS Appl Mater Interfaces 2020;12:44273–80. https://doi.org/10.1021/acsami.0c11062.
[59] Suplicz A, Hargitai H, Kovacs JG. Methodology development for through-plane thermal conductivity prediction of composites. Int J Therm Sci 2016;100:54–9. https://doi.org/10.1016/j.ijthermalsci.2015.09.012.
[60] Xu X, Zhang Q, Hao M, Hu Y, Lin Z, Peng L, et al. Double-negative-index ceramic aerogels for thermal superinsulation. Science 2019;363:723–7. https://doi.org/10.1126/science.aav7304.
[61] Kim P, Doss NM, Tillotson JP, Hotchkiss PJ, Pan M-J, Marder SR, et al. High Energy Density Nanocomposites Based on Surface-Modified $BaTiO_3$ and a Ferroelectric Polymer. ACS Nano 2009;3:2581–92. https://doi.org/10.1021/nn9006412.
[62] Shang Y, Feng Y, Zhang C, Zhang T, Chi Q. Excellent energy storage performance in polymer composites with insulating and polarized two-dimensional fillers. Compos

Part Appl Sci Manuf 2023;167:107429. https://doi.org/10.1016/j.compositesa.2023.107429.
[63] Rasul MG, Kiziltas A, Arfaei B, Shahbazian-Yassar R. 2D boron nitride nanosheets for polymer composite materials. Npj 2D Mater Appl 2021;5:56. https://doi.org/10.1038/s41699-021-00231-2.
[64] Li Y, Cheng S, Zhu Y, Hu J, He J, Li Q. Polymer Nanocomposites with High Energy Density and Breakdown Strength utilizing Oriented BNNS. 2020 IEEE Int. Conf. High Volt. Eng. Appl. ICHVE, Beijing, China: IEEE; 2020, p. 1–4. Doi: 10.1109/ICHVE49031.2020.9279889.
[65] Wang Z, Meng G, Wang L, Tian L, Chen S, Wu G, et al. Simultaneously enhanced dielectric properties and through-plane thermal conductivity of epoxy composites with alumina and boron nitride nanosheets. Sci Rep 2021;11:2495. https://doi.org/10.1038/s41598-021-81925-x.